Atmos. Chem. Phys. Discuss., https://doi.org/10.5194/acp-2018-1164
Manuscript under review for journal Atmos. Chem. Phys.
Discussion started: 4 December 2018

Atmospheric Chemistry and Physics
Discussions
Open Access

Characteristics of atmospheric mercury in East China: implication on sources and formation of mercury species over a regional transport intersection zone

Xiaofei Qin[1], Xiaohao Wang[2], Yijie Shi[1], Guangyuan Yu[1], Yanfen Lin[2], Qingyan Fu[2], Dongfang Wang[2], Zhouqing Xie[3], Congrui Deng[1,*], Kan Huang[1,*]

[1]*Center for Atmospheric Chemistry Study, Shanghai Key Laboratory of Atmospheric Particle Pollution and Prevention (LAP[3]), Department of Environmental Science and Engineering, Fudan University, Shanghai, 200433 China*

[2]*Shanghai Environmental Monitoring Center, Shanghai, 200030 China*

[3]*School of Earth and Space Sciences, University of Science and Technology of China, Hefei, Anhui, 230026 China*

Correspondence: congruideng@fudan.edu.cn, huangkan@fudan.edu.cn

Abstract

Mercury (Hg) is a global pollutant of great concern in East Asia, which is considered to be the largest mercury-emitting region in the world. In this study, atmospheric gaseous elemental mercury (GEM), gaseous oxidized mercury (GOM), and particulate-bound mercury (PBM) were measured continuously over a regional transport intersection zone in East China to reveal the sources and formation of mercury species. The annual mean concentrations of GEM, PBM, and GOM reached 2.77 ng/m^3, 60.80 pg/m^3, and 82.13 pg/m^3, respectively. GEM concentrations were elevated in both cold and warm seasons. This seasonal pattern of GEM suggested that the re-emissions from natural surfaces play a significant role in the fluctuation of atmospheric mercury in addition to anthropogenic sources. Relationship between Hg species and wind directions indicated the high Hg concentrations were related to winds from the south, southwest, and north of the measurement site. An application of the GOM/PBM tracer method and trajectory-based source region identification suggested that long-range transport from northern China and quasi-local emissions were the main sources of Hg species. It was revealed that GEM concentrations were higher when quasi-local sources dominated compared to the dominance of long-range transport events. Six sources and their contributions to anthropogenic GEM were identified. Besides the common anthropogenic emission sectors, shipping emission was found to be an important source (19.6%) of atmospheric mercury in East China, where marine vessel shipping activities are intense. Concurrences of high GOM concentrations with elevated O_3 and temperature, along with the lagged variation of GEM and GOM during daytime demonstrated the very high GOM concentrations were ascribed to the intense in situ oxidation of GEM. Statistical analysis showed that when $PM_{2.5}$ reached a certain value, GOM was inhibited to some extent due to the gas-particle partitioning process. This process was obvious under the conditions of high $PM_{2.5}$ concentrations, high humidity, and low temperature.

1. Introduction

Mercury (Hg) is a global pollutant of great concerns for environment and human health. Based on its physical and chemical properties, atmospheric mercury is operationally divided into three forms, i.e. gaseous elemental mercury (GEM), particulate-bound mercury (PBM), and gaseous oxidized mercury (GOM). GEM is the predominant form in the atmosphere (>90%), while PBM consists of a small quantity of the total mercury as well as for GOM. Elemental mercury in the atmosphere is relatively stable, which means that it has a long lifetime of 0.5-2 year and can transport globally before they are oxidized and removed from the atmosphere via wet and dry depositions (Yu and Luo, 2009). In contrast, GOM and PBM would be rapidly wiped out from the atmosphere after emission due to their significantly greater reactivity, deposition velocities, and water solubility (Yu, 2006;Zhu et al., 2015).

Both natural processes and anthropogenic activities release mercury into the atmosphere. Natural sources of mercury include the ocean volatilization, volcanic eruption, evasion from soils and vegetation, geothermal activities, and weathering minerals (Pirrone et al., 2010;Simoneit et al., 2004). Re-emissions of mercury that previously deposited onto the environmental surfaces are also considered as natural source. As for the anthropogenic mercury, coal combustion, non-ferrous smelters, cement production, waste incineration, and mining are considered to be the main sources. After being emitted into the atmosphere, mercury will experience the chemical and physical speciation and its forms were essential to understand its biogeochemical cycle. Previous studies suggest that the oxidation of GEM in the terrestrial environments was generally initiated by O_3 and OH radicals (Zhang et al., 2013). Atomic bromine (Br) and bromine monoxide (BrO) are two additional oxidation agents in the marine atmosphere (Xiao et al., 2018;Wang et al., 2016).

Observational studies of GOM in the polar regions (Choi et al., 2013;Ye et al., 2016) and in the subtropical marine boundary layer (Cheng et al., 2014;Zhu et al., 2014) as well as atmospheric modeling studies about mercury cycling (Feng et al., 2004;Shon et al., 2005) have considered Br to be an important oxidant of GEM. (Wang et al., 2014) even reported that Br is the primary oxidant of GEM in tropical marine boundary layer (MBL). However, it still remain unknown and controversial about the speciation and quantification of the GEM+O_3 products, and the reaction of GEM+OH is still under huge debate between theoretical and experimental studies due to the lacking of mechanisms consistent with thermochemistry (Xiao et al., 2018). As the GEM converts into GOM, a part of GOM will be adsorbed onto particulate matter since it has high water solubility and relatively strong surface adhesion properties (Liu et al., 2010). GEM accounts for the vast majority of total mercury in the atmosphere, and its concentration is an order of magnitude higher than that of GOM and PBM. Hence, the part of GEM that is lost via the redox reactions might not cause a huge disturbance to its concentration, while the GOM species from the GEM oxidation and subsequent formation of PBM by adsorption on the particle matters can significantly affect their ambient concentrations, especially in regions with high GEM levels.

Many efforts have been made by governments to reduce mercury emissions. In October 2013, 128 countries signed a global treaty “Minamata Convention for mercury” in order to reduce mercury emissions from anthropogenic activities (Zhu et al., 2016). However, the situation of mercury pollution is still grim, especially in Asia, which contribute about half of the global mercury emissions (Wu et al., 2006). Mainland China plays an important role in the biogeochemical cycling of mercury, since about 27% of the global total atmospheric mercury exhausts are from this area (Hui et al., 2017). The Yangtze River Delta (YRD) is one of the most industrialized and urbanized regions in China. Some previous studies showed that the atmospheric mercury pollution in Shanghai is very serious (Friedli et al., 2011;Duan et al., 2017). However, studies with respect to the sources of Hg in East China and the associated formation and transformation processes among Hg species in the atmosphere are still lacking.

In this study, one-year comprehensive measurements of GEM, GOM, and PBM were conducted at Dianshan Lake Station (DSL), a suburban site in Shanghai. DSL is located in the junction of Shanghai, Zhejiang, and Jiangsu provinces and is close to the East China Sea (ECS). Few local sources and multiple surroundings make DSL a unique location for studying the main pollution sources and transport pathways of Hg. In this paper, the relationship between Hg and meteorological conditions was revealed; and the oxidation process of GEM to GOM and the adsorption process of GOM on ambient particles were discussed. We also assessed the potential contributing sources of Hg, locating the high potential sources regions and identifying the specific source and their contributions. This study demonstrated the characteristics of atmospheric mercury over an intersection zone and provided insights into the formation of GOM and PBM, and revealed the considerable contribution from shipping activities over the coastal area.

2. Materials and methods

2.1. Site description

The field observation was conducted on the top of a three-story building at a super site which is located in the west of Shanghai, and nearby the Dianshan Lake in Qingpu district (Fig. 1). DSL lies at suburbs of Shanghai and there are no large point sources around within 20 kilometers. Beside the measurement site is Dianshan Lake, which is the largest freshwater lake in Shanghai with a total area of 62 square kilometers, and next to the site is a highway with moderate traffic. Its special geographical location (at the junction of Shanghai, Zhejiang and Jiangsu provinces) makes it possible to receive the air masses from all these populous regions. In addition, this site is located at the typical outflow path from East China to the Pacific Ocean. The red dots in Fig. 1 represent the amount of atmospheric Hg emitted by anthropogenic activities of each provinces in 2014 (Wu et al., 2016). The emission intensities of anthropogenic Hg in China were higher in the north and lower in the south.

2.2 Measurement of atmospheric mercury species

Atmospheric mercury species (GEM, GOM, and PBM) were collected and measured from June 2015 to May 2016 using the Tekran 2537B/1130/1135 system (Tekran Inc., Canada). The Tekran system has been widely used and the details have been described elsewhere (Landis and Keeler, 2002). In general, GEM, GOM, and PBM in the atmosphere were collected by dual gold cartridges, KCl-coated annular denuder, and regenerable quartz fiber filter, respectively. In this study, GEM was collected at an interval of 5 minutes with a flow rate of 1 L/min, while GOM and PBM were collected at an interval of 2 hours with a flow rate of 10L/min. After the collection, all mercury species were thermally decomposed to Hg^0 immediately and measured by cold vapor atomic fluorescence spectroscopy (CVAFS). GEM concentrations were expressed in ng/m^3, while GOM and PBM were in pg/m^3 at standard temperature of 273.14K and pressure of 1013 hPa. A series of work need to be done to ensure the accuracy and validity of the measurement. The KCl-coated denuder, Teflon coated glass inlet, and impactor plate were replaced weekly and quartz filters were replaced monthly. Before sampling, denuders and quartz filters were prepared and cleaned according to the methods in Tekran technical notes. The Tekran 2537B analyzer was routinely calibrated using its internal permeation source every 47 hours, and was also cross-calibrated every 3 months against an external temperature controlled Hg vapor standard.

2.3 Measurement of other air pollutants and meteorological parameters

Water-soluble inorganic anions (SO_4^{2-}, NO_3^-, Cl^-) and cations (K^+, Mg^{2+}, Ca^{2+}, NH_4^+) in $PM_{2.5}$ were simultaneously monitored by the Monitor for Aerosols and Gases in ambient Air (MARGA) at the resolution of one hour. Ambient air was drawn into a sampling box at a flow rate of 16.7L/min. After removing the water-soluble gases by an absorbing liquid, a supersaturation of water vapor induced the particles in the airflow to grow into droplets, and then the droplets were collected and transported into the analytical box which contains two ion chromatograph systems for the determination of the water-soluble ions in $PM_{2.5}$.

Heavy metals (Pb, Fe, K, Ba, Cr, Se, Cd, Ag, Ca, Mn, Cu, As, Hg, Ni, Zn, V) in $PM_{2.5}$ were measured hourly using the Xact-625 Ambient Metals Monitor (Cooper Environmental services, Beaverton, OR, USA), which is a sampling and analyzing X-ray fluorescence spectrometer designed for online measurements of particulate elements. In this study, ambient air was sampled at a flow rate of 16.7L/min and the particles were collected onto a Teflon filter tape. Then the filter tape was moved into the spectrometer, where it was illuminated with an X-ray tube under three excitation conditions and the excited X-ray fluorescence was measured by a silicon drift detector. Daily advanced quality assurance checks were performed during 30 minutes after midnight to monitor shifts in the calibration.

The hourly meteorological data (air temperature, relative humidity, wind speed, and wind direction) were simultaneously monitored at the observation site by the automatic weather station (AWS). Atmospheric ozone (O_3) concentration was continuously measured using Thermo Fisher

49i, which operates on the principle that ozone molecules absorb UV light at a wavelength of 254 nm. The ambient carbon monoxide (CO) and $PM_{2.5}$ concentrations were measured by Thermo Fisher 48Itle and Thermo Fisher 1405F, respectively.

2.4 Potential source contribution function (PSCF)

PSCF is a useful tool to diagnose the possible source areas with regard to the levels of air pollutants when setting a contamination concentration threshold at the receptor site. Back trajectory models are used to simulate the airflows. The principle of PSCF is to calculate the ratio of the total number of back trajectory segment endpoints in a grid cell (*i*, *j*) which exceed the threshold concentration (m_{ij}) to the total number of back trajectory segment endpoints in this grid cell (*i*, *j*) during the whole sampling period (n_{ij}) as expressed by Equation 1 (Hopke, 2003;Cheng et al., 2015).

$$\mathrm{PSCF}_{ij} = \frac{m_{ij}}{\mathrm{n}_{ij}} \qquad (1)$$

When a particular cell is associated with a small number of endpoint, weighting function (w_{ij}) is applied to reduce this uncertainty and the value of w_{ij} is set as below (Fu et al., 2011).

$$\mathrm{w_{ij}} = \begin{cases} 1.0, & \mathrm{N_{ij}} > 3\mathrm{N_{ave}} \\ 0.7, & 3\mathrm{N_{ave}} > \mathrm{N_{ij}} > 1.5\mathrm{N_{ave}} \\ 0.4, & 1.5\mathrm{N_{ave}} > \mathrm{N_{ij}} > \mathrm{N_{ave}} \\ 0.2, & \mathrm{N_{ave}} > \mathrm{N_{ij}} \end{cases} \qquad (2)$$

In this study, we set the threshold concentration as the mean value of the whole sampling period. Backward trajectories were calculated every two hours and the cell size was set as 0.5°×0.5°.

2.5 Positive matrix factorization (PMF)

The PMF model (Paatero and Tapper, 1994) is widely used to quantitatively determine the source contributions of specific air pollutants. The essential principle behind PMF is that every concentration is determined by source profiles and source contributions to every sample. The equation of the PMF model is shown as Eq. (3):

$$X_{ij} = \sum_{k=1}^{P} g_{ik} f_{kj} + e_{ij} \qquad (3)$$

X_{ij} is the concentration of the *j*th contamination at the receptor site in the ith sample. g_{ik} represent the contribution of the *k*th factor on the *i*th sample, f_{kj} is used to express the mass fraction of the *j*th contamination in the *k*th factor, *P* is the number of factors, which represent pollution sources, e_{ij} is the residual for each measurement or model error.

Before the model determines the optimal non-negative factor contributions and factor profiles, an objective function, which is the sum of the square difference between the measured and modeled concentrations weighted by the concentration uncertainties, has to be minimized (Cheng et al., 2015). The equation that determines the objective function is given by Eq. (4):

$$\mathrm{Q} = \sum_{i=1}^{n} \sum_{j=1}^{m} \left(\frac{X_{ij} - \sum_{k=1}^{p} A_{ik} F_{kj}}{S_{ij}} \right)^2$$

where X_{ij} is the ambient concentration of the *j*th pollutant in the *i*th sample (m and n represent the total number pollutants and samples, respectively). A_{ik} is the contribution of the *k*th factor on the *i*th sample and F_{kj} is the mass fraction of the *j*th pollutant in the *k*th factor. S_{ij} is the uncertainty of the *j*th pollutant on the *i*th measurement, *P* is the number of factors, which imply the pollutant sources.

3. Results and discussion

3.1. Characteristics of atmospheric mercury species

Fig. 2 displays the time series of atmospheric GEM, PBM, and GOM concentrations during 1 June, 2015 to 31 May, 2016 at DSL. The annual average concentrations of GEM, PBM, and GOM at DSL were 2.77 ng/m^3, 60.80 pg/m^3, and 82.13 pg/m^3, respectively. As shown in Table 1, the levels of GEM and PBM in this study were lower than some sites in China by a factor of 2-7, such as rural Miyun, suburban Xiamen, and urban Guiyang (Zhang et al., 2013;Xu et al., 2015;Fu et al., 2011). However, compared to the studies conducted in urban and rural areas abroad such as New York (Choi et al., 2013), Chicago (Gratz et al., 2013), and Nova Scotia (Cheng et al., 2014), the concentrations of GEM and PBM in the suburbs of Shanghai were much higher by a factor of 1-3 and 3-8, respectively. Different from GEM and PBM, the GOM concentrations at DSL were higher than all the Chinese sites and other sites around the world listed in Table 1. The mean GOM concentration in this study (82.13 pg/m^3) was even higher than that in Guiyang (35.7 pg/m^3), where the emissions of GEM and GOM were quite intense due to the massive primary emission sources such as coal-fired power plants and cement plants (Fu et al., 2011). The abnormally high GOM concentrations observed in this study were likely attributed to both strong primary emissions and secondary formation, which will be discussed further in Section 3.4.

The monthly patterns of GEM, PBM, and GOM during the whole sampling period are shown in Fig. 3. The seasonal mean GEM concentrations were slightly higher in winter (2.88 ng/m^3) and summer (2.87 ng/m^3) than in spring (2.73 ng/m^3) and autumn (2.63 ng/m^3), with the highest monthly mean value of 3.19 ng/m^3 in June and the lowest of 2.39 ng/m^3 in March. This seasonal pattern showed the occurrences of high GEM concentrations in both cold and warm seasons, which was different from many urban and remote sites in China, such as Guiyang, Xiamen, and Mt. Changbai, where GEM showed significantly high concentrations in cold seasons than those in warm seasons (Feng et al., 2004;Xu et al., 2015;Fu et al., 2012). The relatively high GEM concentrations during the cold season in this study should be attributed to the increases of energy consumption. In contrast, the elevated GEM concentrations in the warm season likely originated from natural mercury emissions (e.g. soils, vegetations, and water) due to elevated temperature. The seasonal mean PBM concentrations were the highest in winter (93.49 pg/m^3) while the lowest in summer (35.72 pg/m^3), and moderate in autumn (56.75 pg/m^3) and spring (51.63 pg/m^3), with the highest monthly mean value of 109.38 pg/m^3 in January and the lowest of 28.89 pg/m^3 in September. This seasonal pattern was consistent with other sites in China such as Beijing and Nanjing (Zhang et al., 2013;Zhu et al., 2014). PBM concentrations at low altitude sites in the Northern Hemisphere were commonly enhanced in winter, which was ascribed to intense emissions from residential heating, the reduction of wet scavenging processes, enhanced gas-particle partitioning of atmospheric mercury under low temperature, etc. (Rutter and Schauer, 2007). As for GOM, its seasonal mean concentrations were the highest in winter (124.02 pg/m^3), followed by summer (77.27 pg/m^3), spring (68.14 pg/m^3), and autumn (60.95 pg/m^3). The winter maximum of GOM suggested the significant influence of anthropogenic emissions and unfavorable meteorological conditions. The relatively high GOM concentrations in summer indicated that the formation of GOM from GEM oxidation was likely to be crucial.

Fig. 4 shows the diurnal variation of GEM, PBM, and GOM during the whole sampling period. To ensure the time resolutions were consistent among all three mercury species, the temporal resolution of measured GEM was converted from 5 minutes to a two-hour average. As shown in Fig. 4, GEM concentrations were higher during daytime with the maximum in the morning at around 10:00 and minimum in the midnight at around 02:00. The diurnal trends of GOM were as similar as that of GEM, except that the minimum GOM occurred at around 20:00 in the evening. The diurnal trends of PBM were different from those of GEM and GOM, exhibiting relatively higher concentrations during nighttime. The PBM maximum occurred in the early morning at around 6:00 and the minimum was observed in the afternoon at 18:00. The diurnal trends of GEM, PBM, and GOM were as similar as those in Nanjing (Zhu et al, 2012), but different from those in Guiyang, Xiamen, and Guangzhou (Feng et al., 2004;Chen et al., 2013). The elevated GEM concentrations at DSL during daytime were likely related to the stronger emissions from both human activities and natural releases. Apart from direct emissions, high GOM concentrations at daytime partially resulted from in situ GEM oxidation. The high PBM concentrations at night were likely derived from the adsorption of Hg species onto the preexisting particles and the subsequent accumulation in the shallow nocturnal boundary layer. Fig. 4 shows that wind speed was relatively low while high for relative humidity at night, which were conducive to the adsorption of GOM onto the particles.

3.2. Relationship between Hg species and meteorological factors

Fig. 5 shows the relationship between wind direction/speed and atmospheric mercury species. As shown in Fig. 5a, the prevailing wind at DSL during the study period came from the east, accounting for about one-third of all the wind directions. Winds also prevailed from the north with a fraction of 16%. Wind speed from all directions during the study period was mainly in the range of 0-6 m/s, of which wind speed higher than 4 m/s mainly derived from the east. GEM as a function of wind directions showed that the highest GEM concentrations were linked to the winds from the south and southwest with the mean value of 3.92 ng/m^3, while the mean GEM concentration from the other wind sectors was 2.71 ng/m^3 (Fig. 5b). GOM showed similar wind-concentration patterns as GEM. While PBM showed high concentrations from the north/northwest and south/southwest (Fig. 5c &5d). By referring to Fig. 1, the anthropogenic mercury emissions in northern China were generally higher than southern China. Hence, the observation of high atmospheric Hg concentrations from the north was expected. In this regard, the even higher atmospheric Hg concentrations from the south and southeast than from the north cannot be simply explained by anthropogenic emission sources, implying that there must be additional Hg emission sources. (Wang et al., 2016) reported that the Hg concentrations in the surface soils of southern China were generally higher than the northern China. It was possible that emissions from natural sources, such as soils, vegetations and water, might play an important role.

In order to confirm this conjecture, the relationship between temperature and Hg concentrations at DSL was investigated. Seasonal temperature in ascending order was divided into different groups and the corresponding mean Hg concentrations were plotted in Fig. 6. In spring, it was obvious that the GEM concentrations increased as the temperature increased, and when the temperature increased to a certain value, the trends of other season were similar to spring. This relationship between GEM and temperature can only be interpreted as the impact of natural source emissions. It must be noted that the height of PBL increased as the temperature increased, while at the same time, GEM still showed a significant upward trend. This suggested that the atmospheric dilution effect caused by the developing boundary layer was far from offsetting the increase of natural mercury emissions caused by increased temperature. The GOM concentration showed a clearly positive correlation with temperature in summer. This should be related to the in situ oxidation of GEM under high temperature and it will be further discussed in Section 3.4. In the other seasons, no clear correlations between GOM and temperature were observed. As for PBM, it appeared to have weakly negative correlations with the height of PBL, suggesting the atmospheric diffusion conditions were influential on the concentrations of PBM.

3.3. Tracing sources of Hg species

3.3.1. Potential source regions of Hg species

PSCF was applied to identify the potential source regions of the three Hg species. As for GEM, the major source areas were located in Anhui, Jiangxi, and Zhejiang provinces, and there were also signals from Shandong province (Fig. 7a). As for the seasonal pattern (Fig. S1), the potential source regions of GEM in spring were mainly from Jiangsu and Zhejiang provinces. In summer, the PSCF hotspots were identified in Anhui and Jiangxi provinces. Jiangsu province was likely to become the main potential source region of GEM in autumn. In winter, Anhui and Zhejiang provinces showed relatively high PSCF values. In addition, there were also signals from Henan and Shandong provinces, suggesting the importance of long-range transport in wintertime. It was obvious from Fig. 7a that there were substantial high PSCF signals, even stronger than those from the north, from the southern areas. However, as shown in Fig. 1, southern provinces such as Zhejiang and Jiangxi were estimated to release only 25 tons/yr atmospheric Hg from anthropogenic activities, being far less than the northern provinces such as Jiangsu and Shandong (77 tons/yr) (Wu et al., 2016). If only the anthropogenic emissions of GEM were considered, the occurrence of stronger PSCF signals in southern provinces seemed unreasonable. In this regard, the re-emission of GEM from natural surfaces in southern areas should be a crucial source, corroborating the discussion in Section 3.2. In addition, it was found that vast areas of the East China Sea were also identified as potential source regions of GEM in all four seasons (Fig. S1), indicating the non-negligible influence from shipping activities. The detailed estimation of variable sources would be discussed in Section 3.3.3.

The PSCF pattern of PBM was quite different from that of GEM (Fig. 7b). The potential source regions of all year round PBM were mainly from northeastern China, including Jiangsu, Anhui, Shandong, and Hebei provinces. These provinces were regarded as the main Hg sources areas in China and accounted for about 25.2% of the Chinese anthropogenic atmospheric Hg emissions (Wu et al., 2016). As for the seasonal PSCF patterns of PBM (Fig. S2), its potential source regions in spring, autumn, and winter shared certain commonalities that exhibited the consistent PSCF patterns as the annual pattern. The exception was found for summer, which showed high PSCF values mainly in the southern areas of Shanghai. This might be attributed to that the prevailing winds in summer were from the south, southeast, and southwest where Zhejiang and Jiangxi provinces were important mercury source regions.

The potential source regions of all year round GOM were mainly located in Anhui and Zhejiang provinces and the coastal areas along Jiangsu province (Fig. 7c). Compared to the PSCF patterns of GEM and PBM, the potential source regions of GOM were more from southern China rather than from northern China, which might be due to the higher atmospheric oxidants levels in the southern regions. This was most obvious in summer that the potential sources regions of GOM were mainly from Zhejiang and Jiangxi provinces (Fig. S3). In the other seasons, there were somewhat different PSCF patterns observed. In detail, while obvious PSCF signals from the inland areas were found, moderate PSCF signals over the East China Sea and Yellow Sea also observed in spring. In autumn, the high PSCF values mainly occurred in Zhejiang province and there were also moderate signals over the Yellow Sea. In winter, the high PSCF values spread from the coastal areas of Jiangsu to a vast ocean of the Yellow Sea. One previous study suggested that the marine boundary layer could provide considerable amounts of oxidants such as chlorine and bromine, which were beneficial for the production of GOM by oxidizing GEM (Auzmendi-Murua et al., 2014) and this may explain the substantial PSCF signals over the ocean. It should be noted that the signals from the ocean in summer were weaker than in the other seasons. This was likely due to the particularly high ozone concentrations over land in summer (Lu et al., 2018), leading to the formation of GOM dominated by mainland oxidants rather than the ocean oxidants.

The results of the PSCF analysis suggested the significant influences of adjacent areas of Shanghai on contributing to all the atmospheric mercury species. It was also illustrated that the long-range and regional transport via both land transport and sea breeze were important.

3.3.2. Comparison between the impact of quasi-local sources and regional/long-range transport on atmospheric mercury

According to the relationship between wind direction and Hg species as well as the PSCF analysis discussed above, the elevated GEM, GOM, and PBM concentrations at the observation site were generally related to the wind sectors from the southwest and north. In order to reveal the relative importance of local sources and regional transport, the ratio of GOM/PBM was applied as an indicator based on the fact that the residence time of GOM is generally considered to be shorter than that of PBM. If regional/long-range transport was evident, the ratio of GOM/PBM should be lower due to that GOM was more quickly scavenged than PBM during the transport, and vice versa when local sources dominated. In this regard, the ratios of GOM/PBM during the whole study period were grouped into four categories, i.e. 0-1, 1-2, 2-3, and higher than 3. The corresponding frequency of wind direction in each category was compared in Fig. 8. It was clear that the higher GOM/PBM ratios were associated with more frequent winds from the east and southeast. The frequency of these two wind sectors increased significantly from 27% under the GOM/PBM ratios less than 1 to 52% under the GOM/PBM ratios higher than 3. Winds from the east and southeast were typically characterized of relatively clean air masses, suggesting the local sources around the observational site should dominate. In contrast, the lower GOM/PBM ratios were associated with more frequent winds clockwise from the west to the north and the frequency of these wind sectors decreased significantly from 44% under the GOM/PBM ratios less than 1 to 21% under the GOM/PBM ratios higher than 3. These winds were indicative of the long-range/regional transport from northern China and were associated with the relatively low GOM/PBM ratios. According to the PSCF results above, the potential source areas of Hg species (GEM, GOM and PBM) derived mostly from the south and southwest of the sampling site. As shown in Fig. 8, the frequency of south and southwest winds showed no clear trend as the GOM/PBM ratios increased. This suggested the emissions of Hg in the

Atmos. Chem. Phys. Discuss., https://doi.org/10.5194/acp-2018-1164
Manuscript under review for journal Atmos. Chem. Phys.
Discussion started: 4 December 2018

south and southwest of the sampling site were complicated, and the phenomenon above can not be simply explained by the impact of local sources or regional transport.

We further investigated the relationship among GEM, CO, secondary inorganic aerosols (SNA) and GOM/PBM ratios. Fig. 9 displays the concentrations of GEM as a function of GOM/PBM ratios colored by CO. The sizes of the circles represented the corresponding concentrations of SNA in $PM_{2.5}$. CO was commonly used as a tracer of fuel combustion and SNA were derived from secondary formation via the gas-to-particle conversion. CO and SNA were collectively used as proxies of the extent of anthropogenic air pollutants and especially for evaluating the extent of regional/long-range transport. As shown in Fig. 9, GEM showed an overall increasing trend as the GOM/PBM ratios increased. In addition, it could be clearly seen that the lower GOM/PBM ratios were associated with higher CO and SNA concentrations and vice versa. This corroborated the discussion above that the GOM/PBM ratio was a reliable tracer for assessing the relative importance of regional/long-range transport vs. local atmospheric processing.

In the GOM/PBM ratio bins of less than 2.5, GEM fluctuated with the mean values less than 2.6 ng/m^3. The mean GEM concentration increased from 2.61 ng/m^3 in the GOM/PBM ratio bin of 2.5-3.0 to 2.8 ng/m^3 in the bin of 3.0-3.5, and then remain relatively stable when the GOM/PBM ratio bins higher than 3.0. Generally, GEM showed an increasing trend as the GOM/PBM ratios increased while both SNA and CO decreased. The elevation of GEM concentrations tended to be associated with the impact of quasi-local sources. In contrast, under the high SNA and CO conditions when GOM/PBM ratios were lower, GEM was relatively low, suggesting its formation was not favored via the regional/long-range transport. It has been recognized that the common regional/long-range transport pathways on contributing to the particulate pollution events of Shanghai were from the north and northwest originating mostly from the North China Plain. The relatively lower GEM concentrations under the regional/long-range transport conditions corroborated the PSCF analysis that only moderate probabilities of GEM source regions from northern China were found (Fig. 7a).

3.3.3. Source apportionment by PMF

PMF modeling has been widely used to apportion the sources of atmospheric pollutants. In this study, GEM together with heavy metals and soluble ions, measured online synchronously, were introduced into the EPA PMF5.0 model to apportion the major anthropogenic sources of GEM. A six-factor solution was selected based on the results of multiple model runs, which can well explain the measured concentrations of the introduced species. The profiles of six identified PMF factors and contributions of major anthropogenic sources to GEM are shown in Fig. 10. It has to be noted that since no tracers for the natural emissions (e.g. soils, vegetations, and ocean) were available in this study, the identification of natural mercury sources was not possible.

Factor 1 had high loadings for Se, As, Pb, NO_3^-, SO_4^{2-}, and NH_4^+. Se, As, and Pb, which were typical tracers of coal combustion. SO_4^{2-} and NO_3^- were also formed from the gaseous pollutants emitted from coal burning. Hence, this factor was defined as coal combustion sources and accounted for 12.3% of the annual mean GEM.

Factor 2 displayed particularly high loadings for Ni and V. The major sources of Ni in the atmosphere can be derived from coal and oil combustions (Tian et al., 2012), and oil combustion accounted for 85% of anthropogenic V emissions in the atmosphere (Duan and Tan, 2013). In general, Ni and V have been considered as good tracers of heavy oil combustion, which has been commonly used in marine vessels (Viana et al., 2009). Thus, this factor was identified as shipping emissions. The sampling site is adjacent to the East China Sea and is located in Shanghai which has the largest port in the world. It was reasonable that shipping emissions were contributable to the atmospheric Hg, which shouldn't be ignored in the coastal regions. Shipping emissions accounted for 19.6% of GEM and ranked as the second largest emission sector, highlighting the urgent need of controlling the marine vessel emissions.

Factor 3 showed high loadings for Ca and moderate loadings for Ba and Fe. Ca and Fe are rich elements in crust that can be used for cement production. As mercury could be released during industrial processes of cement production, Factor 3 was assigned as cement production and accounted for a minor fraction of 6.3 % of the GEM.

Factor 4 was characterized by high loadings of Cr and moderate loadings of Mn, Fe, Ni, and Cu. These species together served as markers of metals smelting. Metals smelting were known to be large sources of Hg emitted to the atmosphere (Pirrone et al., 2010), especially in the YRD, one of the most developed and industrialized areas in China. This factor accounted for 7.6% of the GEM.

Factor 5 had high loadings of Cl^-. Waste incineration is an important source of enriched chloride over land. We identified Factor 5 to be waste incineration, which contributed 6.4% of the

GEM.

Factor 6 was characterized by high loadings of Cd, Ag, K^+, and Na^+. The major sources of Cd in China were iron and steel smelting industries (Duan and Tan, 2013). Ag was mainly used in industrial applications, including electronic appliances and photographic materials. K^+ was a typical tracer of biomass burning, which often stemmed from agriculture waste burning over the Yangtze River Delta and the North China Plain. In this regard, Factor 6 was considered as a combined source of the industrial and biomass burning emission sectors. It was estimated to contribute 47.8% of the GEM.

3.4. The formation and transformation of mercury species

3.4.1. The formation of GOM

A typical case from July 24 to July 27, 2015 was chosen to investigate the possible formation process of GOM. As shown in Fig. 11, the shaded episodes represented nighttime from 18:00 to 6:00 the next day. It was obvious that both GEM and GOM exhibited rising trends during nighttime (Fig. 11a). This was ascribed to nighttime accumulation effect due to the very shallow boundary layer (Fig. 11c). Starting from 6:00 in the morning, GEM concentrations began to gradually decline as the boundary layer developed. In contrast, the concentrations of GOM continued to rise from 6:00 until it reached the peak value at around 10:00. During this period, the levels of ozone and temperature also kept rising until surpassed 200 $\mu g/m^3$ and 34°C, respectively. Accordingly, as an anthropogenic emitting tracer, the concentration of carbon monoxide was basically stable and even showing a downward trend, which suggested that anthropogenic activities were not the main driving force for the increase of GOM. This phenomenon clearly revealed the acceleration of the conversion process of GEM to GOM under favorable atmospheric conditions of higher O_3 concentration and ambient temperature. In the case of atmosphere dilution by the rise of PBL, the fact that GOM was not falling but rising suggested the great influence of this process on ambient GOM concentrations. Similar observation has been found at the high-altitude Pic du Midi observatory in southern France (Fu et al., 2016), where was almost impervious to anthropogenic emission sources. The important role of GEM oxidation in our sampling site, which located in one of the most developed industrial areas in China, was most likely due to the presence of sufficient oxidants in this area. Severe ozone pollution frequently occurred in the YRD due to strong anthropogenic emission intensities (Lu et al., 2018). Previous studies suggested that the primary oxidants in the terrestrial environment were O_3 and OH radicals (Shon et al., 2005), while Br was an important oxidant in the subtropical marine boundary layer (Obrist et al., 2011). It was possible that, in addition to O_3 and OH radicals, Br might also be an important inducing species to the oxidation of GEM as the DSL site is adjacent to the East China Sea.

Fig. 12 statistically analyzed the relationship among GOM, O_3, and temperature. As similar as Fig. 9, temperature was plotted against a range of GOM/PBM bins colored by O_3 and the size of the circles represented the concentrations of GOM. In general, as temperature and O_3 increased, the concentrations of GOM were subject to substantial enhancement. For instance, when temperature (O_3) was below 12℃ (65.7 μg/m^3), GOM averaged 37.75 pg/m^3. While temperature (O_3) increased to above 20℃ (91.5 μg/m^3), GOM rose to 168.75 pg/m^3, yielding a factor of 1- 5 GOM increases. This further confirmed the case study above that the levels of oxidants under favorable environmental conditions were crucial for the formation of GOM. Fig. 12 also demonstrated the increases of GOM along with the ratios of GOM/PBM. The lower ratios of GOM/PBM were associated with lower temperature and O_3 concentrations, indicating the more probable long-range/regional events during the cold seasons with relatively weak photochemistry. On the contrary, the higher ratios of GOM/PBM were associated with higher temperature and O_3 concentrations, indicating the more probable local events during the warm seasons with relatively strong photochemistry. This suggested that the formation of GOM was more favored by local atmospheric processing rather than the transport. This study demonstrated the abnormally high GOM concentrations observed at DSL were largely ascribed to local oxidation reactions. However, the explicit formation mechanism of GOM need to be investigated by measuring more detailed components of GOM and atmospheric oxidants.

3.4.2. The formation of PBM

Gas-particle partitioning was considered to be an important pathway for the formation of PBM (Amos et al., 2012). Since most of the areas in the YRD belong to non-attainment areas in regard of particulate pollution and the concentrations of GOM were particularly high at DSL as discussed above, the role of gas-particle partitioning in the formation of PBM should be investigated. Fig. 13 shows the statistical pattern of the variation of PBM and GOM in the ascending bins of $PM_{2.5}$. It was obvious that the concentrations of PBM increased with the concentrations of $PM_{2.5}$, which was due to both primary emissions and the subsequent process of Hg species adsorbed on particulate matters. The trend of GOM was somehow different from that of PBM. When $PM_{2.5}$ concentrations were at relatively low levels under 75 μg/m^3, GOM concentrations increased with $PM_{2.5}$. However, when $PM_{2.5}$ concentrations exceeded 75 μg/m^3, GOM exhibited a slightly decreasing trend as $PM_{2.5}$ increased. It seemed that when the concentration of $PM_{2.5}$ reached a certain value, the formation of GOM was inhibited to some extent, which was likely due to the adsorption of GOM onto the particles.

A short episode from December 30, 2015 to January 1, 2016 was chosen to further investigate this phenomenon. As shown in Fig. 14, in Stage 1, the concentrations of $PM_{2.5}$ were below 100 μg/m^3, PBM and GOM shared the similar temporal variation as $PM_{2.5}$. In Stage 2, as $PM_{2.5}$ kept climbing, GOM began to show somewhat negative correlation with $PM_{2.5}$, but not obvious. The reason might be that the relatively high temperature and low humidity during this period were not conducive to the transfer of GOM to particle matters. In Stage 3, GOM decreased as $PM_{2.5}$ continued to increase, showing a clear anti-correlation. During this period, PBM showed a consistent trend with $PM_{2.5}$ and CO. Temperature was relatively low but with relatively high humidity. This phenomenon clearly demonstrated the process of gas-particle partitioning of PBM formation. In stage 4, GOM and PBM showed similar decreasing trend with $PM_{2.5}$ and CO. The low GOM concentrations, low humidity, and high temperature resulted in no significant signs of GOM adsorption to $PM_{2.5}$ in this stage. In general, high $PM_{2.5}$ and GOM concentration in our sampling site made the process of gas-particle partitioning obvious, especially under high humidity and low temperature conditions.

4. Conclusions

In this study, a year-long observation of three atmospheric Hg species was conducted at the Dianshan Lake (DSL) Observatory, located on the typical transport routes from mainland China to the East China Sea. During the whole measurement period, the mean GEM, PBM, and GOM concentrations were 2.77 ng/m^3, 60.8 pg/m^3, and 82.13 pg/m^3, respectively.

Different from many sites in China, GEM at DSL exhibited high concentrations in both warm and cold seasons, which was due to the strong re-emission fluxes from natural surfaces in summer and enhanced coal combustion for residential heating over northern China in winter. The relatively high GOM concentrations in summer indicated that the formation of GOM from GEM oxidation was likely crucial. PBM exhibited high concentrations in winter, indicating the impact from long-range transport. The diurnal patterns of GEM and GOM were similar with relatively high levels during daytime. For GEM, this was likely attributed to both human activities and re-emission from natural surfaces during daytime. For GOM, in addition to direct emissions, high concentrations during daytime were partially ascribed to photochemical oxidation of GEM. The PBM concentrations were higher during nighttime, which was ascribed to the accumulation effect within the shallow nocturnal boundary layer.

The relationship between meteorological factors and atmospheric Hg species showed that the high Hg concentrations were generally related to the winds from the south, southwest, and north and positively correlated with temperature. Both anthropogenic sources and natural sources contributed to the atmospheric mercury pollution at DSL. Higher GOM/PBM ratios corresponded to lower CO and SNA concentrations and vice versa. The ratio of GOM/PBM can be used as a tracer for distinguishing local sources and regional/long-range transport based on the fact that the residence time of GOM was shorter than that of PBM. GEM as a function of the GOM/PBM ratios indicated that when the quasi-local sources dominated, GEM concentrations were relatively higher than those events under the regional/long-range transport conditions. According to the PMF source apportionment results, six sources of GEM and their contributions were identified, i.e. industrial and biomass burning (47.8%), shipping emission (19.6%), coal combustion (12.3%), iron and steel production (7.6%), incineration (6.4%), and cement production (6.3%). The significant contribution of shipping emission suggested that in coastal areas mercury emitted from marine vessels can be significant.

We also investigated the formation processes of GOM and PBM based on episodic studies. The high GOM concentrations were mainly attributed to strong local photochemical reactions under the conditions of high O_3 and temperature. Under high $PM_{2.5}$ concentrations, high humidity and low temperature conditions, the gas-particle partitioning process was obvious at DSL, which might be an important pathway for the formation of PBM.

Data availability. All data used in this study can be requested by contacting the corresponding author (K.H. huangkan@fudan.edu.cn).

Author contributions. KH and CD conceived the study. XQ, KH, and CD wrote the paper. QF, DW, XW, and YL are in charge of the DSL supersite and collected data used in this study. All have contributed to the writing and review of this manuscript.

Competing interests. The authors declare that they have no conflict of interest.

Acknowledgements

This work was supported by the National Key R&D Program of China (Grant Nos. 2018YFC0213105), the Natural Science Foundation of China (NSFC, Grant Nos. 21777029, 91644105), and Environmental Charity Project of Ministry of Environmental Protection of China (201409022).

References

Amos, H. M., Jacob, D. J., Holmes, C. D., Fisher, J. A., Wang, Q., Yantosca, R. M., Corbitt, E. S., Galarneau, E., Rutter, A. P., Gustin, M. S., Steffen, A., Schauer, J. J., Graydon, J. A., St Louis, V. L., Talbot, R. W., Edgerton, E. S., Zhang, Y., and Sunderland, E. M.: Gas-particle partitioning of atmospheric Hg(II) and its effect on global mercury deposition, Atmospheric Chemistry and Physics, 12, 591-603, 10.5194/acp-12-591-2012, 2012.

Auzmendi-Murua, I., Castillo, A., and Bozzelli, J. W.: Mercury Oxidation via Chlorine, Bromine, and Iodine under Atmospheric Conditions: Thermochemistry and Kinetics, Journal of Physical Chemistry A, 118, 2959-2975, 10.1021/jp412654s, 2014.

Chen, L. G., Liu, M., Xu, Z. C., Fan, R. F., Tao, J., Chen, D. H., Zhang, D. Q., Xie, D. H., and Sun, J. R.: Variation trends and influencing factors of total gaseous mercury in the Pearl River Delta-A highly industrialised region in South China influenced by seasonal monsoons, Atmospheric Environment, 77, 757-766, 10.1016/j.atmosenv.2013.05.053, 2013.

Cheng, I., Zhang, L. M., Mao, H. T., Blanchard, P., Tordon, R., and Dalziel, J.: Seasonal and diurnal patterns of speciated atmospheric mercury at a coastal-rural and a coastal-urban site, Atmospheric Environment, 82, 193-205, 10.1016/j.atmosenv.2013.10.016, 2014.

Cheng, I., Xu, X., and Zhang, L.: Overview of receptor-based source apportionment studies for speciated atmospheric mercury, Atmos. Chem. Phys., 15, 7877-7895, 10.5194/acp-15-7877-2015, 2015.

Choi, H. D., Huang, J. Y., Mondal, S., and Holsen, T. M.: Variation in concentrations of three mercury (Hg) forms at a rural and a suburban site in New York State, Sci. Total Environ., 448, 96-106, 10.1016/j.scitotenv.2012.08.052, 2013.

Duan, J., and Tan, J.: Atmospheric heavy metals and Arsenic in China: Situation, sources and control policies, Atmospheric Environment, 74, 93-101, 10.1016/j.atmosenv.2013.03.031, 2013.

Duan, L., Wang, X., Wang, D., Duan, Y., Cheng, N., and Xiu, G.: Atmospheric mercury speciation in Shanghai, China, Sci. Total Environ., 578, 460-468, https://doi.org/10.1016/j.scitotenv.2016.10.209, 2017.

Feng, X. B., Shang, L. H., Wang, S. F., Tang, S. L., and Zheng, W.: Temporal variation of total gaseous mercury in the air of Guiyang, China, J. Geophys. Res.-Atmos., 109, 10.1029/2003jd004159, 2004.

Friedli, H. R., Arellano, A. F., Geng, F., Cai, C., and Pan, L.: Measurements of atmospheric mercury in Shanghai during September 2009, Atmospheric Chemistry and Physics, 11, 3781-3788, 10.5194/acp-11-3781-2011, 2011.

Fu, X., Marusczak, N., Heimbürger, L.-E., Sauvage, B., Gheusi, F., Prestbo, E. M., and Sonke, J. E.: Atmospheric mercury speciation dynamics at the high-altitude Pic du Midi Observatory, southern France, Atmospheric Chemistry and Physics, 16, 5623-5639, 10.5194/acp-16-5623-2016, 2016.

Fu, X. W., Feng, X. B., Qiu, G. L., Shang, L. H., and Zhang, H.: Speciated atmospheric mercury and its potential source in Guiyang, China, Atmospheric Environment, 45, 4205-4212, 10.1016/j.atmosenv.2011.05.012, 2011.

Fu, X. W., Feng, X., Shang, L. H., Wang, S. F., and Zhang, H.: Two years of measurements of atmospheric total gaseous mercury (TGM) at a remote site in Mt. Changbai area, Northeastern China, Atmospheric Chemistry and Physics, 12, 4215-4226, 10.5194/acp-12-4215-2012, 2012.

Gratz, L. E., Keeler, G. J., Marsik, F. J., Barres, J. A., and Dvonch, J. T.: Atmospheric transport of speciated mercury across southern Lake Michigan: Influence from emission sources in the Chicago/Gary urban area, The Science of the total environment, 448, 84-95, 10.1016/j.scitotenv.2012.08.076, 2013.

Hopke, P. K.: Recent developments in receptor modeling, J. Chemometr., 17, 255-265, 10.1002/cem.796, 2003.

Hui, M. L., Wu, Q. R., Wang, S. X., Liang, S., Zhang, L., Wang, F. Y., Lenzen, M., Wang, Y. F., Xu, L. X., Lin, Z. T., Yang, H., Lin, Y., Larssen, T., Xu, M., and Hao, J. M.: Mercury Flows in China and Global Drivers, Environmental science & technology, 51, 222-231, 10.1021/acs.est.6b04094, 2017.

Landis, M. S., and Keeler, G. J.: Atmospheric mercury deposition to Lake Michigan during the Lake Michigan Mass Balance Study, Environmental science & technology, 36, 4518-4524, 10.1021/es011217b, 2002.

Liu, B., Keeler, G. J., Dvonch, J. T., Barres, J. A., Lynam, M. M., Marsik, F. J., and Morgan, J. T.: Urban-rural differences in atmospheric mercury speciation, Atmospheric Environment, 44, 2013-2023, 10.1016/j.atmosenv.2010.02.012, 2010.

Lu, X., Hong, J., Zhang, L., Cooper, O. R., Schultz, M. G., Xu, X., Wang, T., Gao, M., Zhao, Y., and Zhang, Y.: Severe Surface Ozone Pollution in China: A Global Perspective, Environmental Science & Technology Letters, 10.1021/acs.estlett.8b00366, 2018.

Obrist, D., Tas, E., Peleg, M., Matveev, V., Fain, X., Asaf, D., and Luria, M.: Bromine-induced oxidation of mercury in the mid-latitude atmosphere, Nat. Geosci., 4, 22-26, 10.1038/ngeo1018, 2011.

Paatero, P., and Tapper, U.: Positive matrix factorization - a nonnegative factor model with optimal utilization of error-estimates of data values, Environmetrics, 5, 111-126, 10.1002/env.3170050203, 1994.

Pirrone, N., Cinnirella, S., Feng, X., Finkelman, R. B., Friedli, H. R., Leaner, J., Mason, R., Mukherjee, A. B., Stracher, G. B., Streets, D. G., and Telmer, K.: Global mercury emissions to the atmosphere from anthropogenic and natural sources, Atmos. Chem. Phys., 10, 5951-5964, 10.5194/acp-10-

5951-2010, 2010.

Rutter, A. P., and Schauer, J. J.: The effect of temperature on the gas-particle partitioning of reactive mercury in atmospheric aerosols, Atmospheric Environment, 41, 8647-8657, 10.1016/j.atmosenv.2007.07.024, 2007.

Shon, Z. H., Kim, K. H., Kim, M. Y., and Lee, M.: Modeling study of reactive gaseous mercury in the urban air, Atmospheric Environment, 39, 749-761, 10.1016/j.atmosenv.2004.09.071, 2005.

Simoneit, B. R. T., Elias, V. O., Kobayashi, M., Kawamura, K., Rushdi, A. I., Medeiros, P. M., Rogge, W. F., and Didyk, B. M.: Sugars - Dominant water-soluble organic compounds in soils and characterization as tracers in atmospheric particulate matter, Environmental science & technology, 38, 5939-5949, 10.1021/es0403099, 2004.

Tian, H. Z., Lu, L., Cheng, K., Hao, J. M., Zhao, D., Wang, Y., Jia, W. X., and Qiu, P. P.: Anthropogenic atmospheric nickel emissions and its distribution characteristics in China, Sci. Total Environ., 417, 148-157, 10.1016/j.scitotenv.2011.11.069, 2012.

Viana, M., Amato, F., Alastuey, A., Querol, X., Moreno, T., Garcia Dos Santos, S., Dolores Herce, M., and Fernandez-Patier, R.: Chemical Tracers of Particulate Emissions from Commercial Shipping, Environmental science & technology, 43, 7472-7477, 10.1021/es901558t, 2009.

Wang, F., Saiz-Lopez, A., Mahajan, A. S., Martin, J. C. G., Armstrong, D., Lemes, M., Hay, T., and Prados-Roman, C.: Enhanced production of oxidised mercury over the tropical Pacific Ocean: a key missing oxidation pathway, Atmospheric Chemistry and Physics, 14, 1323-1335, 10.5194/acp-14-1323-2014, 2014.

Wang, X., Lin, C.-J., Yuan, W., Sommar, J., Zhu, W., and Feng, X.: Emission-dominated gas exchange of elemental mercury vapor over natural surfaces in China, Atmospheric Chemistry and Physics, 16, 11125-11143, 10.5194/acp-16-11125-2016, 2016.

Wu, Q., Wang, S., Li, G., Liang, S., Lin, C. J., Wang, Y., Cai, S., Liu, K., and Hao, J.: Temporal Trend and Spatial Distribution of Speciated Atmospheric Mercury Emissions in China During 1978-2014, Environmental science & technology, 50, 13428-13435, 10.1021/acs.est.6b04308, 2016.

Wu, Y., Wang, S. X., Streets, D. G., Hao, J. M., Chan, M., and Jiang, J. K.: Trends in anthropogenic mercury emissions in China from 1995 to 2003, Environmental science & technology, 40, 5312-5318, 10.1021/es060406x, 2006.

Xiao, M., Wang, Q., Qin, X., Yu, G., and Deng, C.: Composition, Sources, and Distribution of PM2.5 Saccharides in a Coastal Urban Site of China, Atmosphere, 9, 274, 10.3390/atmos9070274, 2018.

Xu, L. L., Chen, J. S., Yang, L. M., Niu, Z. C., Tong, L., Yin, L. Q., and Chen, Y. T.: Characteristics and sources of atmospheric mercury speciation in a coastal city, Xiamen, China, Chemosphere, 119, 530-539, 10.1016/j.chemosphere.2014.07.024, 2015.

Ye, Z., Mao, H., Lin, C. J., and Kim, S. Y.: Investigation of processes controlling summertime gaseous elemental mercury oxidation at midlatitudinal marine, coastal, and inland sites, Atmos. Chem. Phys., 16, 8461-8478, 10.5194/acp-16-8461-2016, 2016.

Yu, F.: From molecular clusters to nanoparticles: second-generation ion-mediated nucleation model, Atmospheric Chemistry and Physics, 6, 5193-5211, 2006.

Yu, F., and Luo, G.: Simulation of particle size distribution with a global aerosol model: contribution of nucleation to aerosol and CCN number concentrations, Atmospheric Chemistry and Physics, 9, 7691-7710, 2009.

Zhang, L., Wang, S. X., Wang, L., and Hao, J. M.: Atmospheric mercury concentration and chemical speciation at a rural site in Beijing, China: implications of mercury emission sources, Atmospheric

Chemistry and Physics, 13, 10505-10516, 10.5194/acp-13-10505-2013, 2013.

Zhu, J., Wang, T., Talbot, R., Mao, H., Yang, X., Fu, C., Sun, J., Zhuang, B., Li, S., Han, Y., and Xie, M.: Characteristics of atmospheric mercury deposition and size-fractionated particulate mercury in urban Nanjing, China, Atmospheric Chemistry and Physics, 14, 2233-2244, 10.5194/acp-14-2233-2014, 2014.

Zhu, J., Wang, T., Bieser, J., and Matthias, V.: Source attribution and process analysis for atmospheric mercury in eastern China simulated by CMAQ-Hg, Atmos. Chem. Phys., 15, 8767-8779, 10.5194/acp-15-8767-2015, 2015.

Zhu, W., Lin, C. J., Wang, X., Sommar, J., Fu, X., and Feng, X.: Global observations and modeling of atmosphere–surface exchange of elemental mercury: a critical review, Atmos. Chem. Phys., 16, 4451-4480, 10.5194/acp-16-4451-2016, 2016.

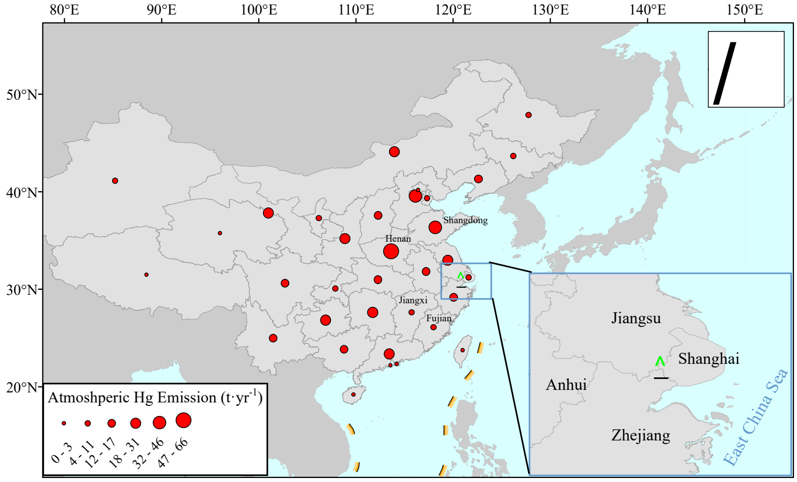

Figure 1. The location of the Dianshan Lake (DSL) site in Shanghai, China. The red dots in the map represent the anthropogenic atmospheric Hg emissions by each province in 2014 (Wu et al., 2016).

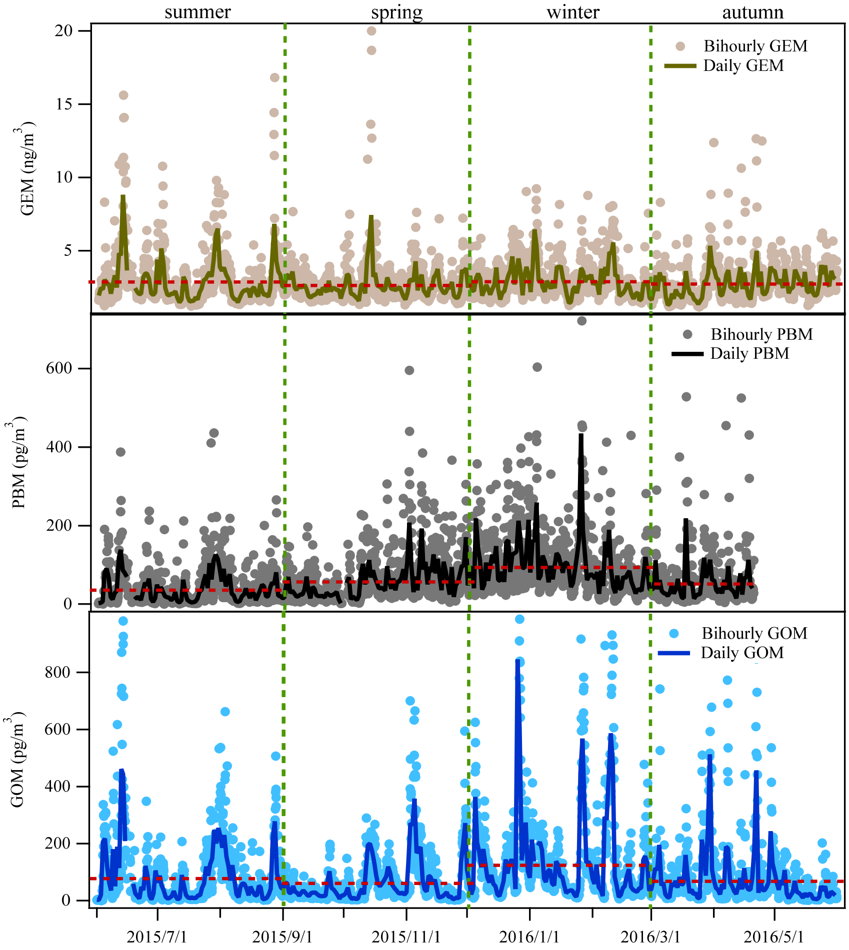

Figure 2. Time series of atmospheric Hg (GEM, PBM and GOM) concentrations during the whole study period at DSL.

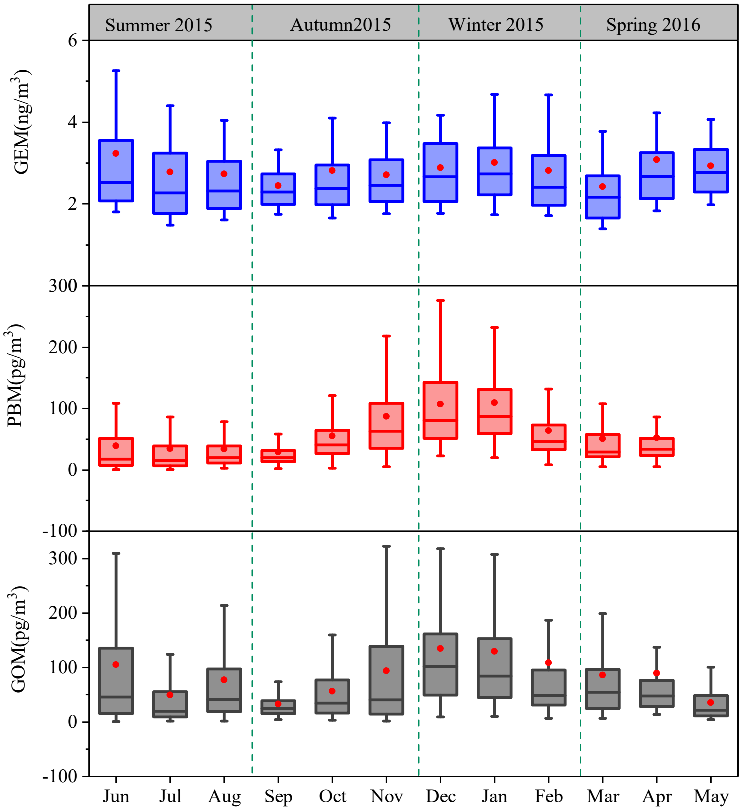

Figure 3. Monthly variation of GEM, PBM, and GOM concentrations. The 10th，25th, median, 75th and 90th percentile values are indicated in the box plots. The red dots represent the mean values.

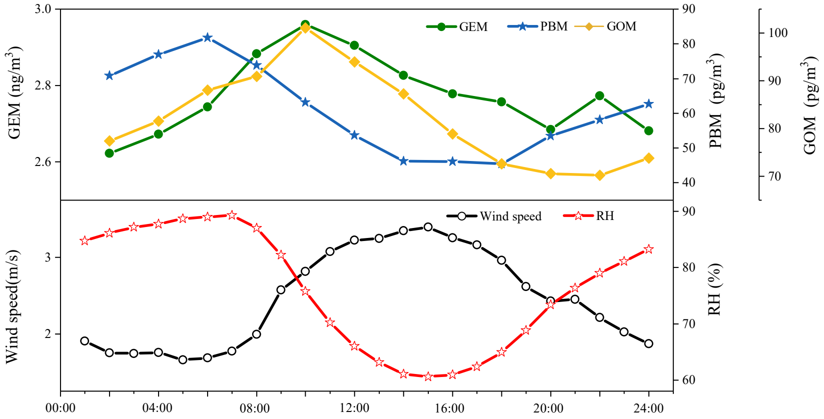

Figure 4. Annual mean diurnal variation of GEM, PBM, and GOM concentrations. The red line and black line represented the corresponding diurnal variation of RH and wind speed, respectively.

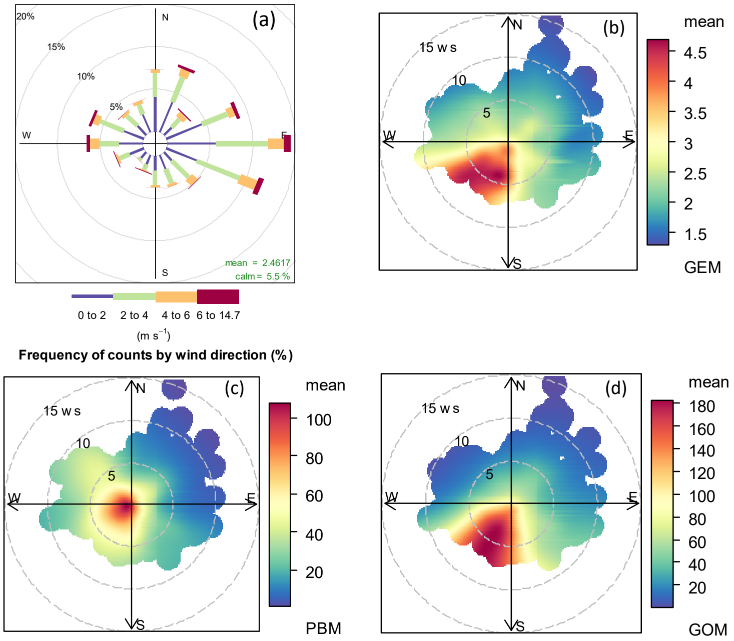

Figure 5. (a) Wind rose plot during the study period. Mean concentrations of (b) GEM, (c) PBM, and (d) GOM as a function of wind speed and wind directions.

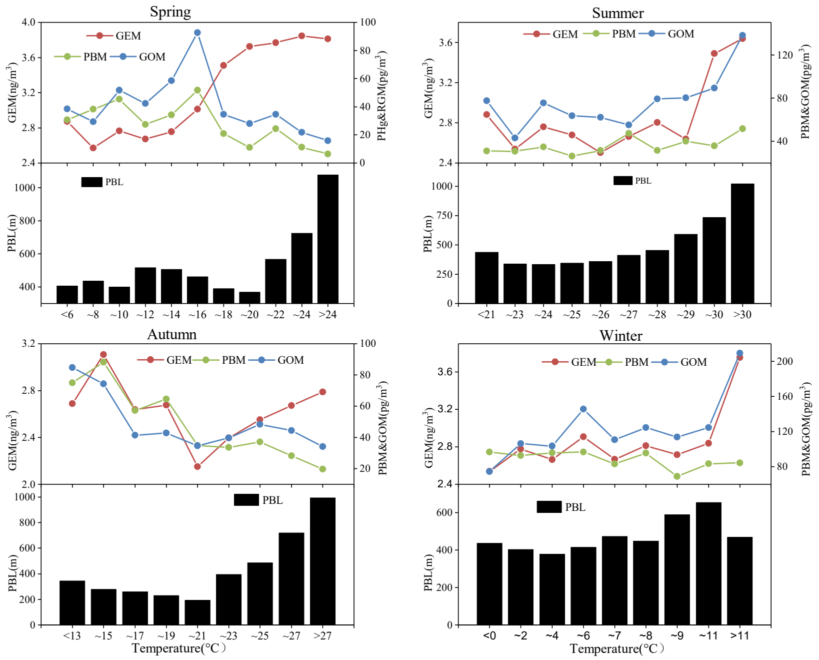

Figure 6. The variation of atmospheric Hg (GEM, PBM, and GOM) and PBL as a function of temperature in all four seasons.

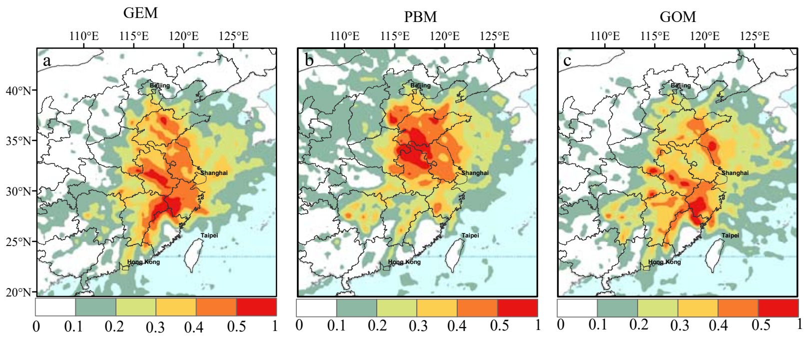

Figure 7. Potential source regions of atmospheric Hg (GEM, PBM and GOM) at the observational site according to PSCF analysis.

Atmos. Chem. Phys. Discuss., https://doi.org/10.5194/acp-2018-1164
Manuscript under review for journal Atmos. Chem. Phys.
Discussion started: 4 December 2018

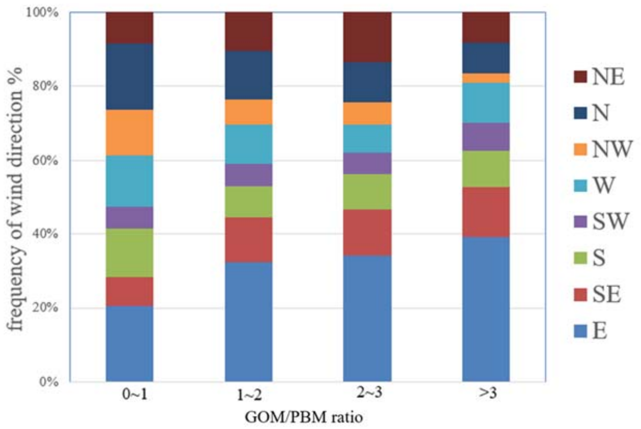

Figure 8. Frequency of wind directions under different ranges of GOM/PBM ratios.

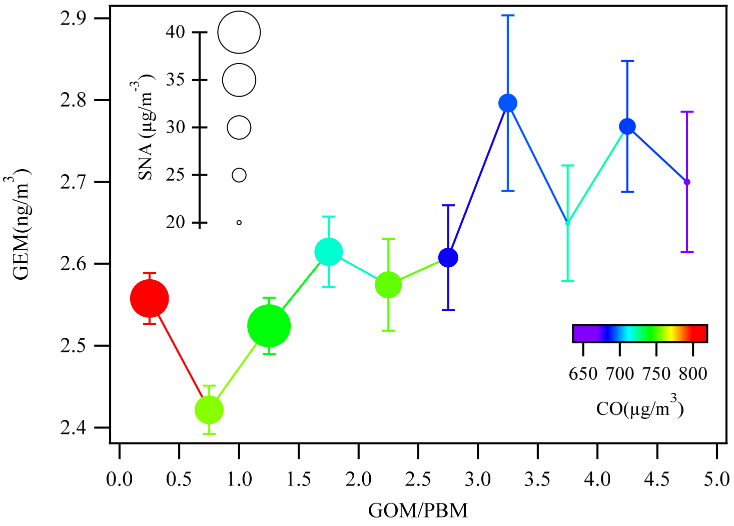

Figure 9. The GEM concentrations as a function of the GOM/PBM ratios in each bin of 0.5. The dots are colored by the concentrations of CO and the sizes of the dots represent the concentrations of SNA (sulfate, nitrate, and ammonium) in $PM_{2.5}$.

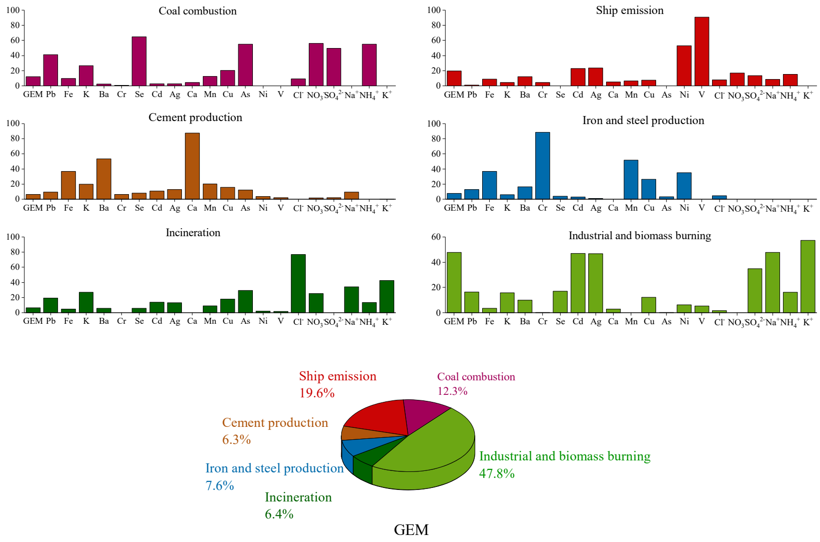

Figure 10. A six factor source apportionment for anthropogenic GEM based on PMF analysis.

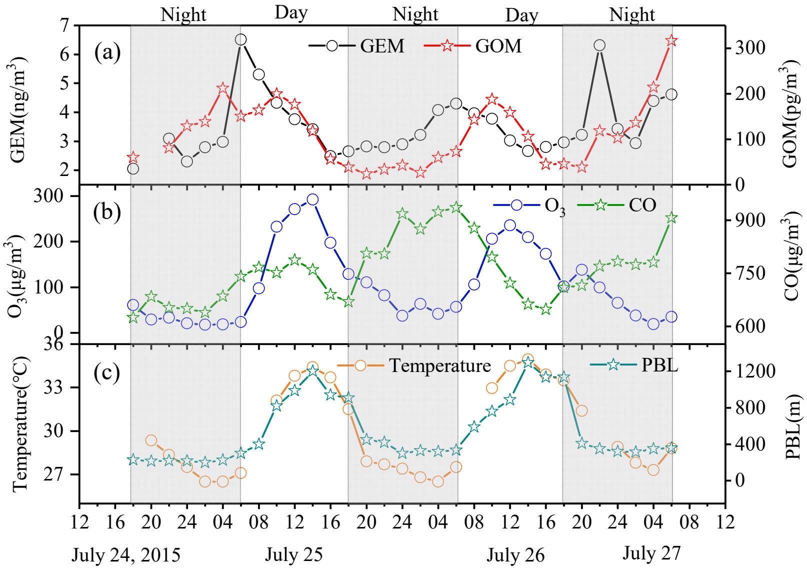

Figure 11. A case study of GEM oxidation from July 24 to 27, 2015. The time-series of GEM, GOM, O$_3$, CO, temperature, and PBL are plotted. The shaded parts represent nighttime.

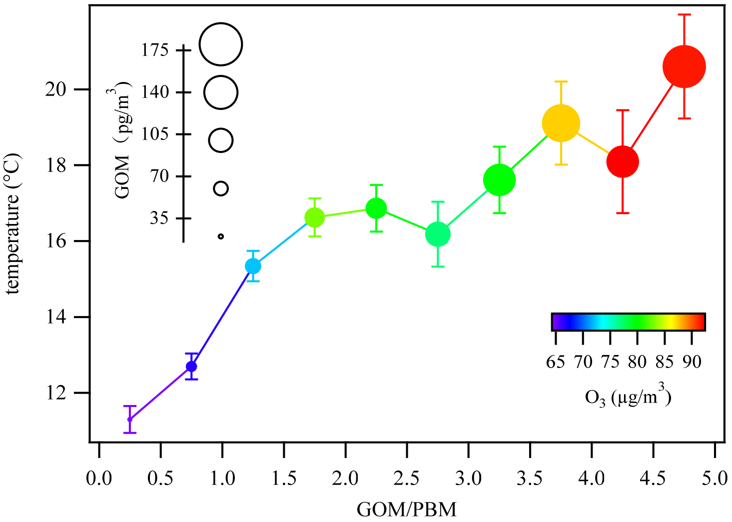

Figure 12. Temperature as a function of the GOM/PBM ratios in each bin of 0.5. The dots are colored by the concentrations of O_3 and the sizes of the dots represent the concentrations of RGM.

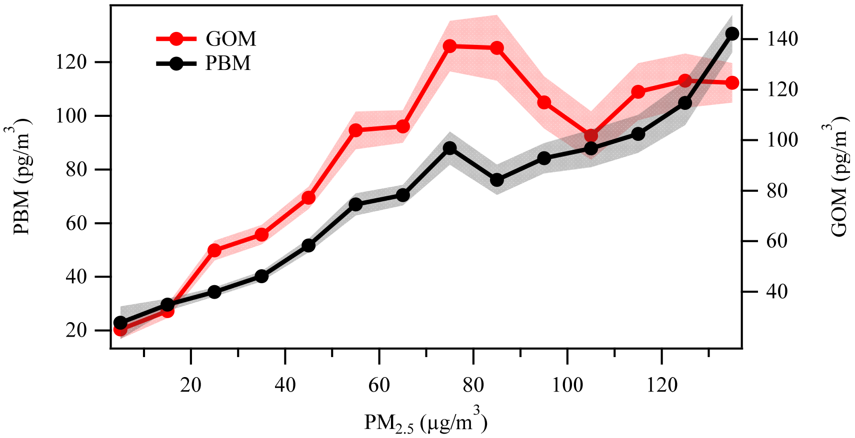

Figure 13. The variations of PBM and GOM as a function of PM$_{2.5}$ in each bin of 10 µg/m^3.

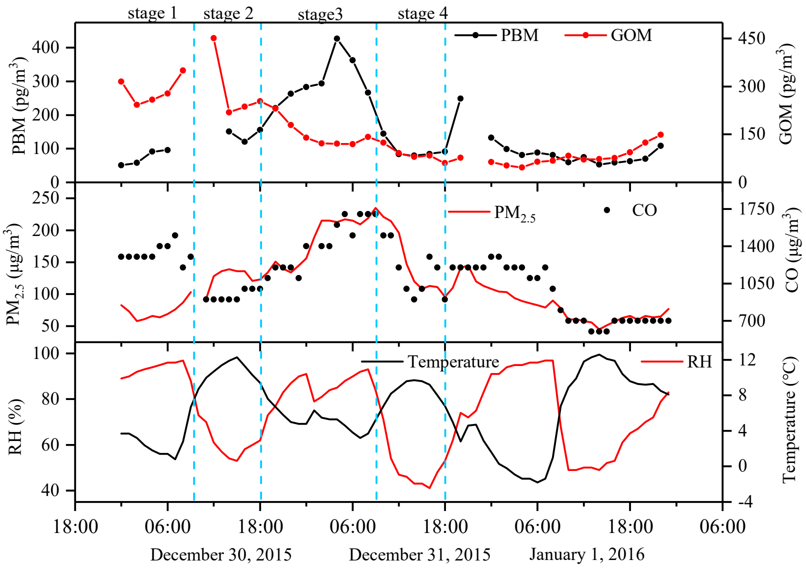

Figure 14. A case study of gas-particle portioning between GOM and PBM from December 30, 2015 to January 1, 2016, which was divided into different stages. The time-series of PBM, GOM, PM$_{2.5}$, CO, temperature, and RH are plotted.

Table 1. The concentrations of speciated atmospheric mercury in this study and other sites around the world.

Location	Remarks	Year	GEM (ng/m^3)	PHg (pg/m^3)	RGM (pg/m^3)	Reference
Dianshan Lake Shanghai, CN	Suburban	2015-2016	2.77±1.36	60.8±67.4	82.13±115.46	This study
Chongming Shanghai, CN	Suburban	2009-2012	2.65±1.73	21.5±25.4	8.0±8.8	Zhang et al. (2017)
Xiamen, CN	Suburban	2012-2013	3.5	174.41	61.05	Xu et al. (2015)
Guiyang, CN	Urban	2009	9.72±10.2	368±676	35.7±43.9	Fu et al. (2011)
Miyun, CN	Rural	2008-2009	3.23	98.2	10.1	Zhang et al. (2013)
Mt.Waliguan, CN	Remote	2007-2008	1.98±0.98	19.4±18.1	7.4±4.8	Wan et al. (2009)
Seoul, Korea	Urban	2005-2006	3.22±2.10	23.9±19.6	27.2±19.3	Kim et al. (2009)
Nova Scotia, Canada	Rural	2010-2011	1.38±0.2	0.4±1.0	3.5±4.5	Cheng et al. (2014)
Elora,Ontario, Canada	Rural	2006-2007	1.17	16.40	15.1	Baya and Van Heyst (2010)
Chicago, USA	Urban	2007	2.5±1.5	9±20	17±87	Gratz et al. (2013)
Reno,USA	Suburban	2007-2009	2.0±0.7	7±7	18±22	Lyman and Gustin (2009)
Rochester, NY, USA	Urban	2008-2009	1.49	6.57	4.08	Huang et al. (2010)